ELSEVIER

Catalysis Today 38 (1997) 23–30

CATALYSIS TODAY

The liquid phase hydrogenation of benzene and substituted alkylbenzenes over a nickel catalyst in a semi-batch reactor

Sami Toppinen[a], Tiina-Kaisa Rantakylä[b], Tapio Salmi[c,*], Juhani Aittamaa[a]

[a] *Neste Engineering, Box 310, FIN-06101 Borgå, Finland*
[b] *Department of Process Engineering, University of Oulu, FIN-90570 Oulu, Finland*
[c] *Åbo Akademi, Laboratory of Industrial Chemistry, FIN-20500 Åbo, Finland*

Abstract

The liquid phase hydrogenation kinetics of benzene, toluene, ethylbenzene and cumene was studied in a three-phase semi-batch reactor at pressures of 20–40 bar and at temperatures of 95–140°C. The experimental kinetics was described with a rate equation based on rapid adsorption and desorption steps and slow consecutive hydrogen steps.

A pseudo-homogeneous model neglecting the diffusion resistances in the catalyst particles was able to phenomenologically describe the observed kinetics, but numerical simulations showed that there exist significant concentration gradients in the particles. Therefore a complete dynamic heterogeneous model was developed for the reactor and the catalyst particles including the reaction–diffusion process. The kinetic parameters were re-determined using the heterogeneous reaction–diffusion model. The model enables the investigation of the reaction–diffusion effects and the dynamics of the catalyst particles.

Keywords: Alkylbenzenes; Hydrogenation; Kinetics; Reaction–diffusion dynamics

1. Introduction

The kinetics of solid catalyzed gas–liquid reactions is traditionally measured in semi-batch slurry reactors, where the finely dispersed catalyst particles are vigorously agitated together with the gas and the liquid phases. The liquid phase is in batch, whereas the gas is either flowing continuously through the reaction mixture or is added to the reaction vessel and the total pressure in the reactor is carefully controlled. The benefit of the slurry reactor is the absence of heat and mass transfer limitations inside the crushed catalyst: the small particle sizes are regarded as a guarantee for the absence of concentration gradients in the particles. The drawbacks with the small particles are the liquid–solid separation problems in the sampling for chemical analysis and the agitation of the mixture. With large catalyst particles the separation problem is avoided and the mixture can be efficiently agitated with magnetic stirrers and by using stagnant or spinning baskets for the catalysts.

The open question in the use of larger catalyst particles is, of course, the role of internal heat and mass transfer in the observed kinetics. Furthermore, the dynamics of the reaction–diffusion process in the catalyst particles should be compared with the dynamics of the bulk phase processes (gas–liquid–solid mass and heat transfer; the bulk phase balances),

*Corresponding author.

PII S0920-5861(97)00035-7

in order to justify the simplifications, for instance, the pseudo-steady-state hypothesis for the catalyst particles. According to our opinion, the necessary tools do exist today for making reliable comparisons of the velocities of different processes being present in a three-phase system. The overall kinetics can be experimentally measured with larger catalyst particles; the mass and heat transfer parameters can be estimated a priori and incorporated in the complete reactor model and the parameters of the intrinsic kinetics can be estimated from the experimental data. The dynamics of the catalyst particles can then be investigated by numerical simulations. The aim of the present work is to demonstrate the usefulness of the procedure described above. The liquid phase hydrogenation of benzene and some alkylbenzenes, especially toluene, was chosen as the demonstration system.

2. Experimental

The experimental work was performed in an automatic semi-batch three-phase reactor system of Xytel B.V. Europe. The total volume of the reactor was 1000 ml. The catalyst particles (Crosfield, 16.6 w% Ni on Al_2O_3) were placed in a static basket, whereas the liquid phase was stirred with a magnetic coupling. Hydrogen was supplied semi-batchwise to the reactor maintaining an approximately constant pressure. Chemicals of analytical grade were used in all the experiments. The catalyst was activated at atmospheric pressure under hydrogen flow prior to the dearomatization experiment. The experiments were performed at a total pressure of 20 and 40 bar and at temperatures of 95°C, 125°C and 140°C. Samples were automatically withdrawn from the liquid phase and analyzed by gas chromatography. The reaction products were identified with gas chromatography–mass spectrometry (GC–MS). Further experimental details are described by Rantakylä [5] and Toppinen [9]. Typical experimental data are presented in Fig. 2.

3. Kinetic model for hydrogenation

The reaction mechanism and the rate equations for the catalytic hydrogenation of aromatic compounds are treated in detail in the previous publications of our group (see, e.g., Ref. [8]). Therefore just the general principles of the mechanism and the final rate equations are reviewed here. The rate equation was based on a mechanistic scheme implying competitive adsorption of organic molecules and hydrogen on the active metal sites (*), consecutive hydrogenation steps on the catalyst surface and product desorption steps. The mechanism is summarized as follows:

$$H_2 + \gamma^* \rightleftarrows \gamma H^*_{2/\gamma} \quad \text{I}$$
$$A + * \rightleftarrows A^* \quad \text{II}$$
$$A^* + \gamma H^*_{2/\gamma} \rightleftarrows AH^*_2 + \gamma^* \quad \text{III}$$
$$AH^*_2 + \gamma H^*_{2/\gamma} \rightleftarrows AH^*_4 + \gamma^* \quad \text{IV}$$
$$AH^*_4 + \gamma H^*_{2/\gamma} \rightleftarrows AH^*_6 + \gamma^* \quad \text{V}$$
$$AH^*_6 \rightleftarrows AH_6 + * \quad \text{VI}$$

where γ is the stoichiometric coefficient of hydrogen adsorption ($\gamma = 1$ for non-dissociative adsorption or $\gamma = 2$ for dissociative adsorption). The adsorption steps I–II were assumed to be rapid, which implies that the quasi-equilibrium hypothesis is applicable for those steps. The product desorption step VI was presumed to be rapid and irreversible. The hydrogenation steps III–V were assumed to be rate determining. These hypotheses led to the primary form of the rate equation which was further simplified by approximating the rate constants of steps III–V to be equal ($= k$) and neglecting the backward rate constants of these steps. The result was the very simple rate expression

$$R = \frac{kK_A K_H c_A c_H}{(3K_A c_A + (K_H c_H)^{1/\gamma} + 1)^{\gamma+1}} \quad (1)$$

where K_A and K_H denote the adsorption equilibrium constants of the aromatic molecule and hydrogen, respectively. For the sake of simplicity, the adsorption parameters were assumed to be temperature-independent, whereas the rate constant was presumed to obey the law of Arrhenius.

4. Reactor model

The following basic assumptions were used in the modelling of the three-phase semi-batch reactor:

- The liquid and gas phases in the reactor are completely backmixed because of vigorous agita-

tion. Thus temperature and concentration gradients can appear inside the catalyst particle only.

- The mass and heat transfer at the gas–liquid interphase is described with the two-film theory and with Fick's law.
- The mass and heat transfer limitations at the outer surfaces of the catalyst particles are neglected.
- The mass and heat transfer resistances inside the catalyst particles are described with effective heat conductivities and with effective diffusion coefficients.
- Thermodynamic equilibria are assumed to prevail at the gas–liquid interphase. The local phase equilibria are described with the Soave–Redlich–Kwong equation of state.
- The catalyst particle is presumed to be completely wetted; thus the reaction proceeds as a liquid phase process and the contribution of gas phase hydrogenation is ignored.
- The surface processes (adsorption, surface reaction and desorption) on the catalyst are assumed to be in quasi-steady-state. Thus the Langmuir–Hinshelwood-type of rate equations (1) are applicable.
- The models for the bulk phases and the catalyst particles are dynamic, including the accumulation terms for heat and mass. The energy balances for the bulk phases were not included in the model because the reactor temperature was continuously recorded during the course of the experiment and these data were directly incorporated in the model.

Based on these assumptions, the reactor model can be written as follows. For a component in the liquid bulk we have

$$\frac{dn_{Li}}{dt} = N_{GLi}A - N_{LSi}A_P \tag{2}$$

where N_{GLi} and N_{LSi} denote the fluxes from the gas phase to the liquid phase and from the liquid phase into the catalyst particle, respectively; A and A_P are the corresponding surface areas and dn_{Li}/dt accounts for the accumulation term in the bulk liquid. The processes are illustrated in the schematic picture (Fig. 1). Analogously, we can write for the gas bulk the component mass balance.

$$\frac{dn_{Gi}}{dt} = -N_{GLi}A + F_i \tag{3}$$

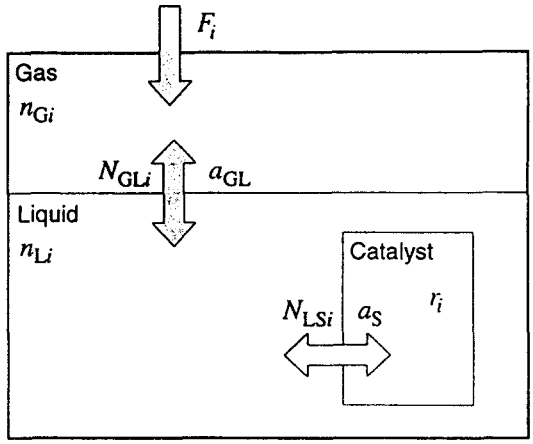

Fig. 1. Schematic picture of the reactor and the transport processes.

where F_i is the feed into the gas phase ($F_i = 0$ except for H_2) and dn_{Gi}/dt describes the accumulation in the gas phase. The hydrogen feed F_{H_2} was described by simulating a proportional controller. After introducing mass transfer area-to-reactor volume ratios ($a = A/V_R$ and $a_P = A_P/V_R$) and some rearrangements the mass balances become

$$\frac{dn_{Li}}{dt} = (N_{GLi}a - N_{LSi}a_P)V_R \tag{4}$$

$$\frac{dn_{Gi}}{dt} = -N_{GLi}aV_R + F_i \tag{5}$$

The fluxes at the gas–liquid interphase (N_{GLi}) are obtained from the two-film theory and Fick's law. The details are discarded here; the final expression becomes

$$N_{GLi} = \frac{c_{Gi}/K_i' - c_{Li}}{1/k_{Gi}aK_i' + 1/k_{Li}a} \tag{6}$$

where $k_{Gi}a$ and $k_{Li}a$ denote the volumetric mass transfer coefficients for gas and liquid, respectively. The gas–liquid equilibrium ratio K_i' for component i is obtained from the corresponding thermodynamic equilibrium ratio (K_i) and the total concentrations in the phases:

$$K_i' = \frac{K_i c_{Gtot}}{c_{Ltot}} \tag{7}$$

The concentrations in the gas and liquid phases were obtained from the amounts of substance and the phase

volumes; for example, for the liquid phase according to the procedure

$$c_{Li} = n_{Li}/V_L \tag{8}$$

where

$$V_L = \frac{\Sigma n_{Li} M_i}{\rho_L} \tag{9}$$

An analogous approach was applied on the gas phase.

The fluxes at the solid–liquid interphase depend on the concentration gradients at the outer surface ($r = R_P$) of the catalyst particles. A local mass balance gives

$$N_{LSi} A_P = D_{ei} \left(\frac{dc_{Li}}{dr} \right)_{r=R_P} A_P \tag{10}$$

The gradients at the surface are obtained from the solution of the mass balances for the catalyst particles.

After applying the standard balance considerations to the cylindrical catalyst particles we obtain the dynamic mass and energy balance equations

$$\frac{dc_i}{dt} = \frac{D_{ei}}{\varepsilon_P} \left(\frac{d^2 c_i}{dr^2} + \frac{1}{r} \frac{dc_i}{dr} \right) + \rho_P \nu_i R \tag{11}$$

$$\frac{dT}{dt} = \frac{\lambda_P}{\rho_P c_p} \left(\frac{d^2 T}{dr^2} + \frac{1}{r} \frac{dT}{dr} \right) + \frac{(-\Delta H_r)}{c_p} R \tag{12}$$

where R is the hydrogenation rate, ν_i is the stoichiometric coefficient and ΔH_r is the reaction enthalpy. The other symbols are explained in the Notation.

The boundary conditions of Eqs. (11) and (12) are trivial; for the centerline (at $r = 0$):

$$dc_i/dr = 0 \tag{13}$$

$$dT/dr = 0 \tag{14}$$

and for the outer surface ($r = R_P$):

$$c_i = c_{Li} \tag{15}$$

$$T = T_L \tag{16}$$

The mathematical model consists of coupled ordinary differential equations (ODEs), Eqs. (4) and (5) for the bulk phases and parabolic partial differential equations (PDEs) Eqs. (11) and (12) for the catalyst particles, respectively. A self-evident numerical solution stragegy comprises the conversion of the PDEs to ODEs with respect to time, and the solution of the created ODEs as an initial value problem with respect to time (t). The space derivatives (dc_i/dr, d^2c_i/dr^2, $dT/dr\, d^2T/dr$) were discretized with central difference formulae (e.g., a five-point formula for d^2c_i/dr^2) and the ODE system formed was solved with the backward difference method [3] using the software LSODE [4].

The numerical solution of the model was implemented as subroutines for the parameter estimation, which was performed with the software KINFIT [10] using an adaptive non-linear least squares algorithm NL2SOL [2]. The experimentally measured quantities were the weight fractions of the aromatic compound (w_A). Thus the weight fraction predicted from the model (w_A) was calculated from

$$w_A = \frac{x_A M_A}{\Sigma x_i M_i} \tag{17}$$

where the mole fractions are

$$x_i = \frac{c_{Li}}{c_L} \tag{18}$$

The objective function (Q) in the parameter estimation was defined as

$$Q = \Sigma (w_{\exp A,j} - w_{A,j})^2 \tag{19}$$

where the subscript expAJ denotes the different experimental points (see, e.g., Fig. 2).

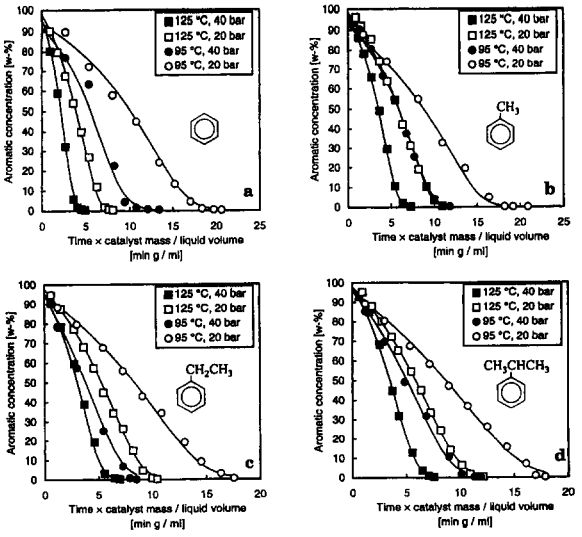

Fig. 2. Experimental and predicted kinetic curves for the hydrogenation of benzene and some alkylbenzenes.

Table 1
Physical properties of the catalyst

R_P	Efficient radius	0.25 mm
ε_P	Porosity	0.5
λ_P	Heat conductivity	0.15 W/(k K)
ρ_P	Density	1300 kg/m^3
τ_P	Tortuosity	4.0

5. Physical properties

The densities (i.e., molar volumes) of the gas and liquid phases were estimated with the Soave–Redlich–Kwong equation of state [6] using the data bank of the process simulator Flowbat [1]. The same equation of state was also used in the estimation of the fugacity coefficients which give the equilibrium ratios (Eq. (7)). The effective diffusion coefficients, D_{ei}, were calculated from the relation

$$D_{ei} = \frac{\varepsilon_P}{\tau_P} D_i \tag{20}$$

where ε_P and τ_P denote the porosity and tortuosity of the catalyst pellet, respectively, and D_i is the molecular diffusion coefficient. D_i was calculated from the binary diffusion coefficients using the approximation of Wilke [6]. The binary diffusion coefficients were obtained from the Wilke–Chang equation [11]. The other physical properties were partly based on measurements and partly on approximate values found in the literature [7]. A summary of these parameters is given in Table 1.

Rigorous thermodynamic calculations indicated that the reaction enthalpy is virtually independent of the temperature in the actual conditions. Therefore a constant value of $\Delta H_r = -210$ kJ/mol was used in the calculations for all alkylbenzenes.

6. The dynamics of reaction kinetics and diffusion in catalyst particles

The kinetic and adsorption parameters were first determined for a pseudo-homogeneous version of the model, that is, neglecting the heat and mass transfer parameters inside the catalyst particle. The parameter values of the pseudo-homogeneous model are given elsewhere [9] and they are therefore not repeated here. The fit of the pseudo-homogeneous kinetic model to the experimental data was excellent; the model predictions followed closely the experimental aromatic concentrations.

Table 2
Estimated kinetic parameters

Parameter	B	MB	EB	IPB
$k(T_0)$, mol/(kg s)	1.3	2.1	5.2	5.6
E_a, kJ/mol	54	20	23	19
10^4 K_A, m^3/mol	18	2.5	1.3	1.1
10^3 K_H, m^3/mol	> 7000	37	3.9	2.1

$T_0 = 373.15$ K.
B = benzene.
MB = methylbenzne (toluene).
EB = ethylbenzene.
IPB = isopropylbenzene (cumene).

A preliminary simulation of the concentration profiles inside the catalyst particle, using the parameters of the pseudo-homogeneous model indicated, however, that intraparticle mass transfer resistance might be of importance. Therefore, the parameter estimation was repeated with the complete heterogeneous model, that is, Eqs. (4)–(16). The parameters obtained for the heterogeneous model are listed in Table 2. An example of the fit of the model to the primary data is shown in Fig. 2. De facto the fit was not improved by the shift from the homogeneous to the heterogeneous model, but the correctness of the heterogeneous model can be validated by studying the concentration and temperature profiles inside the catalyst particles.

Two important questions are raised in the consideration of the concentration and temperature profiles in the catalyst particles. Firstly, does there exist any concentration and temperature gradients in the particle in pseudo-steady-state conditions (i.e., gradients for the case $dc_i/dt = 0$ and $dT/dt = 0$ in Eqs. (11) and (12)); and secondly, how rapidly is the pseudo-steady state established in the particles, that is, is it justified to use the pseudo-steady-state approximation for the catalyst particle.

An example of the pseudo-steady-state temperature profile in the particle is shown in Fig. 3 ($p_{H_2} = 40$ bar, $T = 125$°C). The conditions in the figure correspond to the initial conditions of the experiment. It is clearly observable that the temperature gradients in the particle are of very minor importance, even though the reaction is highly exothermic. The calculated

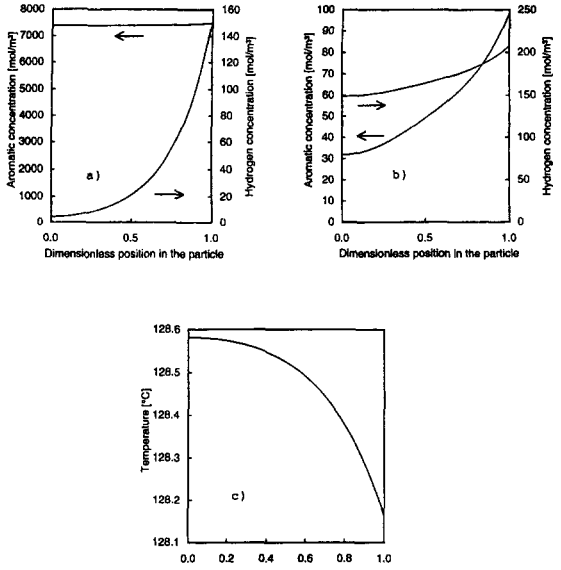

Fig. 3. Pseudo-steady-state concentration (a,b) and temperature (c) profiles in the catalyst particle at 40 bar and 125°C. The cases: (a) and (c); the beginning of the experiment (90 wt.% toluene); (b); the end of the experiment (2 wt.% toluene).

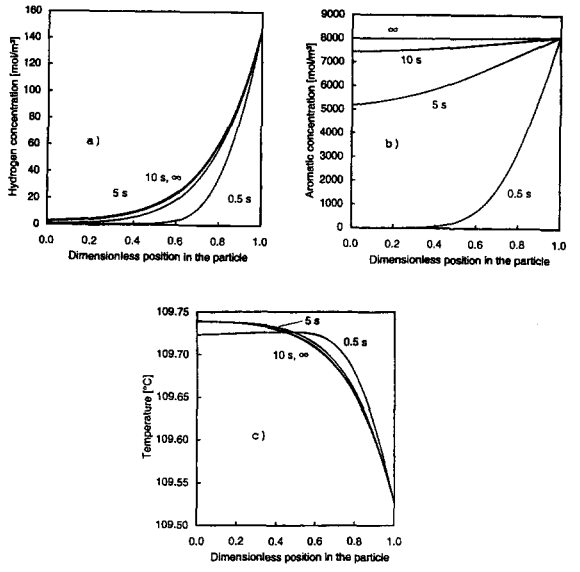

Fig. 4. The dynamics of the concentration (a,b) and temperature (c) profiles in the catalyst particle in the hydrogenation of toluene.

temperature difference between the centre and the surface of the particle was always less than 1°C. For the concentration profiles the situation is completely different as demonstrated in Fig. 3(a) and (b), which show the pseudo-steady-state concentration profiles in the beginning (Fig. 3(a)) and at the end (Fig. 3(b)) of the experiment. For both cases the hydrogen concentration varies significantly within the particle. In the beginning of the experiment the hydrogen concentration decreases practically to zero in the centre of the particle, which implies that the inner part of the particle is not used at all in the hydrogenation. Probably the most internal parts of the catalyst are in a deactivated state, since the surface is covered by the aromatic compound.

At the beginning of the experiment, the concentration gradient of the aromatic compound is negligible as can be seen from Fig. 3a. We can thus conclude that the diffusion resistance of the aromatic compound is negligible at the beginning of the experiment. Intuitively it would be expected that the diffusion resistance of the aromatic compound could be ignored throughout the experiment. Fig. 3b shows, however, that this is not the case: significant concentration gradients of toluene exist inside the particle at the final stage of the experiment. The internal parts of the particle are for this case dominated by the saturated product molecule. Summa summarum: it is necessary to use the heterogeneous reaction–diffusion model not only for hydrogen but also for the armoatic compound and the hydrogenated product.

In the following stage, the dynamics of the development of the concentration and temperature profiles were investigated with numerical simulations. The results of the simulations are summarized in Fig. 4a–c. The figures demonstrate that the dynamics of the intraparticle process are orders of magnitude faster than the dynamics of the overall reaction: the reaction times in the experiments were several hours (Fig. 2). The dynamic simulations show that a pseudo-steady state is established inside the particle within few seconds; the temperature and hydrogen concentration profiles are stabilized during the first 10 s of the experiment; the aromatic concentration profile requires slightly more time to stabilize because the aromatic molecule is larger and it has thus a smaller diffusion coefficient than hydrogen. However, the aromatic concentration profile also attains its pseudo-steady state during the first minute of the experiment. (Fig. 4b).

7. Conclusions

The study showed that the liquid phase hydrogenation of benzene and alkylbenzenes is strongly dominated by intraparticle mass transfer resistance in the commercial catalyst particles; the governing factor is the mass transfer resistance of hydrogen, but the mass transfer of the aromatics also play a role, particularly at high conversions, at the end of the hydrogenation.

Furthermore, the simulation of the particle dynamics showed that a pseudo-steady state model for the particles is physically sufficient for the hydrogenation in semi-batch conditions, since the reactor dynamics itself is much slower than the diffusion process inside the particle. For numerical calculations it is, however, beneficial to use the set of the completely dynamic Eqs. (4) and (5) and Eqs. (11) and (12). The results presented here were obtained for toluene as a model molecule, but our studies with benzene and with other alkylbenzenes, for example, the xylenes, isopropylbenzene, cumene and mesitylene, indicate that the conclusions can be generalized to the entire family of substituted alkylbenzenes.

8. Notation

a	surface area-to-reactor volume ratio
A	surface area
c	concentration
c_p	heat capacity
D	molecular diffusion coefficient
D_e	effective diffusion coefficient
E_a	activation energy
F	feed rate
ΔH_r	reaction enthalpy
k	rate constant
K	equilibrium or adsorption constant
M	molar mass
n	amount of substance
N	flux
Q	objective function
p	pressure
r	radial coordinate in the catalyst particle
R	reaction rate
R_P	radius of the catalyst particle
t	time
T	temperature
T_0	average temperature of the experiments
V	volume
w	weight fraction
x	mole fraction
ε_P	porosity of the catalyst particle
γ	stoichiometric coefficient for hydrogen adsorption
λ_P	heat conductivity of the catalyst particle
ν	stoichiometric coefficient
ρ	density
ρ_P	density of the catalyst particle
τ_P	tortuosity of the catalyst particle

8.1. *Subscripts and superscripts*

A	aromatic component
G	gas
GL	gas–liquid (interphase)
H	hydrogen
i	component index
j	index for an experimental point
L	liquid
LS	liquid–solid (interphase)
P	catalyst particle
tot	total concentration
*	active site

References

[1] J.J. Aittamaa, Flowbat, User's Manual, Neste Engineering, Porvoo, Finland (1994).
[2] J.E. Dennis, D.M. Gay and R.E. Welsch, An adaptive nonlinear least-squares algorithm, ACM Trans. Math. Software, 7 (1982) 369–383.
[3] P. Henrici, Discrete Variable Methods in Ordinary Differential Equations. Wiley, New York, NY (1962).
[4] A.C. Hindmarsh, ODEPACK, A systematized collection of ODE solvers, Scientific Computing, North Holland, Amsterdam, (1983) 55–64.
[5] T. Rantakylä, Lic. Technol. Thesis, University of Oulu, Oulu, Finland (1996).
[6] R.C. Reid, J.M. Prausnitz, B.E. Poling, The Properties of Gases and Liquids, McGraw-Hill, New York, NY (1987).
[7] C.N. Satterfield, Mass Transfer in Heterogeneous Catalysis MIT Press, Cambridge, MA (1970).

[8] S. Smeds, D. Murzin and T. Salmi, Kinetics of ethylbenzene hydrogenation on Ni/Al_2O_3, Appl. Catal. A, 125 (1995) 272–291.

[9] S. Toppinen, Doctoral thesis, Åbo Akademi, Åbo, Finland, (1996).

[10] S. Toppinen, KINFIT – A program package for parameter estimation (private communication), (1996).

[11] C.R. Wilke and P. Chang, Correlation of diffusion coefficients in dilute solutions, AIChE J., 1 (1955) 264–270.